INTERNATIONAL JOURNAL FOR NUMERICAL AND ANALYTICAL METHODS IN GEOMECHANICS
Int. J. Numer. Anal. Meth. Geomech., 2006; **30**:1213–1230
Published online 12 May 2006 in Wiley InterScience (www.interscience.wiley.com). DOI: 10.1002/nag.523

A novel analytical solution for constant-head test in a patchy aquifer

Shaw-Yang Yang[1] and Hund-Der Yeh[2,*,†]

[1] *Department of Civil Engineering, Vanung University, Chungli, Taiwan*
[2] *Institute of Environmental Engineering, National Chiao Tung University, Hsinchu, Taiwan*

SUMMARY

A mathematical model describing the hydraulic head distribution for a constant-head test performed in a well situated at the centre of a patchy aquifer is presented. The analytical solution for the mathematical model is derived by the Laplace transforms and the Bromwich integral method. The solution for the hydraulic head has been shown to satisfy the governing equations, related boundary conditions, and continuity requirements for the hydraulic head and flow rate at the interface of the patch and outer regions. An efficient numerical approach is proposed to evaluate the solution, which has an integral covering an integration range from zero to infinity and an integrand consisting the product and square of the Bessel functions. This solution can be used to produce the curves of dimensionless hydraulic head against dimensionless time for investigating the effect of the contrast of formation properties on the dimensionless hydraulic head distribution. Define the ratio of outer-region transmissivity to patch-region transmissivity as α. The dimensionless hydraulic head for $\alpha = 0.1$ case is about 2.72 times to that for $\alpha = 10$ case at dimensionless large time (e.g. $\tau \geqslant 10^6$) when the dimensionless distance (ρ) equals 10. The results indicate that the hydraulic head distribution highly depends on the hydraulic properties of two-zone formations.

Received 7 August 2004; Revised 15 August 2005; Accepted 2 December 2005

KEY WORDS: constant-head test; patchy aquifer; analytical solution; numerical approach

1. INTRODUCTION

The determination of hydraulic parameters through an aquifer test is commonly used in site characterization. The constant-flux and constant-head tests are two different kinds of aquifer tests. The former requires maintaining a constant well discharge (or injection) and measure the

*Correspondence to: Hund-Der Yeh, Institute of Environmental Engineering, National Chiao Tung University, 75, Po-Ai St., Hsinchu, Taiwan.
†E-mail: hdyeh@mail.nctu.edu.tw

Contract/grant sponsor: Taiwan National Science Council; contract/grant number: NSC90-2621-Z-009-003

drawdowns at observation wells. The constant-head test is frequently carried out in a single well for which a constant head must be maintained in order to measure the transient flow rate across the wellbore. The constant-head test is suitable to use in the low-permeability formations for estimating aquifer parameters.

An aquifer having a small region of anomalous hydrogeological properties may be called a well in a cylindrical inhomogeneity (patchy aquifer). A patchy aquifer may have the radius of heterogeneous cylinder (patchy region) up to 60 m [1] and can be considered as a composite aquifer system. During well construction, a wellbore skin of finite thickness may be developed due to the invasion of drilling mud into the adjacent formation or the removal of fine particles from the surrounding formation by extensive well development; consequently, the original homogeneous aquifer may become a composite aquifer system also. In any case, the thickness of skin zone may range from a few millimeters to several meters, and thus must be considered in pumping-test-data analyses [2]. Barker and Herbert [1] gave a Laplace-domain solution for the problem of a well pumped with a constant rate and situated at the centre of disc of a patchy aquifer. Actually, the aquifer is generally of low transmissivity in the patch region and of relatively high transmissivity in the outer region under most field conditions [1, 2]. Concepts of the infinitesimal and finite-thickness regions with a heterogeneous property in contrast to that of the outer region are commonly used to investigate the effect of the patch region on the result of well constant-head tests. Streltsova [3, 4] considered an infinitesimal heterogeneous aquifer and used the skin factor to represent the heterogeneous aquifer effect. Novakowski [5] developed a Laplace-domain solution for the transient flow rate across the wellbore for composite aquifers with considering the effects of the finite-thickness heterogeneous aquifer and well partial penetration. Curves of dimensionless hydraulic head versus dimensionless time were developed to investigate the influences of the finite-thickness heterogeneous aquifer and well partial penetration on the hydraulic head distribution. Markle *et al*. [6] developed a model for composite aquifer with a partially penetrating well that has a finite-thickness heterogeneous aquifer and intersects a single vertical fracture. Their results show that the finite-thickness heterogeneous aquifer and the well partial penetration can affect the transient flow rate across the wellbore. For a constant-head test in a radial composite aquifer system, Chang and Chen [7] gave the Laplace-domain solutions for the hydraulic heads and flow rate across the wellbore. However, their solution for the head distribution in an undisturbed aquifer is incorrect. In this study, we derive a closed-form solution (i.e. time-domain solution) to describe the hydraulic head distribution for a constant-head test in a patchy aquifer with a fully penetrating well. The solution is expressed in an integral form that has an integration range from zero to infinity. The integral is difficult to evaluate due to the integrand not only consisting of the product and square of the Bessel functions, but also having a singularity at the origin. Therefore, we present a numerical approach including a root-search scheme, the Gaussian quadrature, and the Shanks method to evaluate this solution. This approach is in a very efficient way when evaluating the solution. Finally, the effects of hydrogeological properties and thickness of the patch region on dimensionless hydraulic head distribution are explored. In addition, for dealing with the problem of the well constant-head test, this new solution can be used as a fundamental tool for testing and benchmarking numerical codes, performing sensitivity analysis for model parameters, and even identifying the hydrogeological properties when coupling with an optimization algorithm in the test-data analyses.

DOI: 10.1002/nag

2. PROBLEM STATEMENT

2.1. Groundwater flow equations

A patchy aquifer system with a well for pumping tests is depicted in Figure 1. The confined aquifer consists of two regions with transmissivities T_1 for $r_w \leqslant r \leqslant r_1$ in the patch region and T_2 for $r \geqslant r_1$ in the outer region. Assumptions made for the confined-aquifer solution are: (1) the aquifer is homogeneous, isotropic, and has infinite-extent with a constant thickness, (2) the well is fully penetrated with a finite radius, and (3) the initial hydraulic head is constant and uniform throughout the whole aquifer. Using these assumptions, the equations which express the combination of mass balance and Darcy's law through the patch and outer regions are, respectively,

$$\frac{\partial^2 h_1}{\partial r^2} + \frac{1}{r}\frac{\partial h_1}{\partial r} = \frac{S_1}{T_1}\frac{\partial h_1}{\partial t}, \quad r_w \leqslant r \leqslant r_1 \tag{1}$$

and

$$\frac{\partial^2 h_2}{\partial r^2} + \frac{1}{r}\frac{\partial h_2}{\partial r} = \frac{S_2}{T_2}\frac{\partial h_2}{\partial t}, \quad r_1 \leqslant r < \infty \tag{2}$$

where the subscripts 1 and 2, respectively, denote the patch region around the wellbore and the outer region, h is the hydraulic head distribution, T is the transmissivity, S is the storage coefficient, r is the radial distance from the centre of well, r_w is the radius of well, r_1 is the outer radius of the patch region (or the cylinder radius of the patch region), and t is the time from the start of test. These two equations represent the hydraulic heads within the patch and outer regions, respectively.

The hydraulic heads are initially assumed to be zero within both the patch and outer regions, that is

$$h_1(r, 0) = h_2(r, 0) = 0 \quad \text{for } r > r_w \tag{3}$$

As r approaches infinity, the derivative of hydraulic head with respect to the radial distance tends to zero. Such a boundary condition for the outer region may be specified as

$$\frac{\partial h_2(\infty, t)}{\partial r} = 0 \tag{4}$$

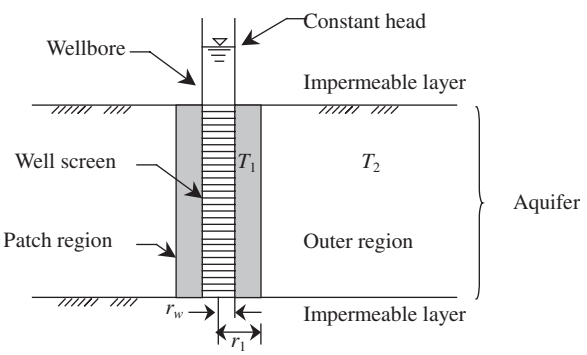

Figure 1. Schematic diagram of the well and patchy aquifer configurations.

DOI: 10.1002/nag

The boundary condition for maintaining a constant head at $r = r_w$ is given by

$$h_1(r_w, t) = h_w \tag{5}$$

where h_w is the constant head around the wellbore at any time.

The continuities of hydraulic head and flow rate at the interface of the patch and outer regions, respectively, require

$$h_1(r_1, t) = h_2(r_1, t) \tag{6}$$

and

$$T_1 \frac{\partial h_1(r_1, t)}{\partial r} = T_2 \frac{\partial h_2(r_1, t)}{\partial r} \tag{7}$$

2.2. Derivation of closed-form solutions

Applying the Laplace transform on (1) and (2) subject to the initial condition (3), the solutions of the transformed governing equations with four unknown constant can be obtained. Similarly, the transformed boundary conditions of (4)–(7) can be obtained when taking the Laplace transform. The Laplace-domain solutions in the patch and outer regions can then be obtained by substituting the transformed boundary conditions into the solutions of the transformed governing equations subsidiary formulas. The results of $\bar{h}_1$ and $\bar{h}_2$ expressed for the patch and outer regions are, respectively,

$$\bar{h}_1 = \frac{h_w}{p} \frac{\phi_1 I_0(q_1 r) - \phi_2 K_0(q_1 r)}{\phi_1 I_0(q_1 r_w) - \phi_2 K_0(q_1 r_w)} \tag{8}$$

and

$$\bar{h}_2 = \frac{h_w}{p} \frac{-K_0(q_2 r)}{[r_1 q_1][\phi_1 I_0(q_1 r_w) - \phi_2 K_0(q_1 r_w)]} \tag{9}$$

where $q_1^2 = pS_1/T_1$, $q_2^2 = pS_2/T_2$, p is the Laplace variable [8], $I_0(\cdot)$ and $K_0(\cdot)$ are, respectively, the modified Bessel functions of the first and second kinds of order zero, and

$$\phi_1 = \sqrt{\frac{S_2 T_2}{S_1 T_1}} K_0(q_1 r_1) K_1(q_2 r_1) - K_1(q_1 r_1) K_0(q_2 r_1) \tag{10}$$

and

$$\phi_2 = \sqrt{\frac{S_2 T_2}{S_1 T_1}} I_0(q_1 r_1) K_1(q_2 r_1) + I_1(q_1 r_1) K_0(q_2 r_1) \tag{11}$$

where $I_1(\cdot)$ and $K_1(\cdot)$ are the modified Bessel functions of the first and second kinds of order one, respectively. Note that the solutions of (8) and (9) were also given by Chang and Chen [7]. However, their hydraulic head in the outer region is slightly different from (9). They gave a term $r_1 q_2$, instead of $r_1 q_1$, in the denominator of hydraulic head in the outer region.

The time-domain solutions of (8) and (9) obtained by employing the method of the Bromwich integral [9] are

$$h_1 = h_w + \frac{2h_w}{\pi} \int_0^\infty e^{-(T_1/S_1)u^2 t} \frac{[A_1(u, r)B_2(u) - A_2(u, r)B_1(u)]}{[B_1^2(u) + B_2^2(u)]} \frac{du}{u} \tag{12}$$

DOI: 10.1002/nag

and

$$h_2 = h_w - \frac{4h_w}{\pi^2 r_1}\int_0^\infty e^{-(T_1/S_1)u^2 t}\frac{[J_0(\kappa r u)B_1(u) + Y_0(\kappa r u)B_2(u)]}{[B_1^2(u) + B_2^2(u)]}\frac{du}{u^2} \tag{13}$$

where

$$A_1(u,r) = \sqrt{\frac{S_2T_2}{S_1T_1}}[J_0(r_1u)Y_1(\kappa r_1 u)Y_0(ru) - Y_0(r_1u)Y_1(\kappa r_1 u)J_0(ru)] - [J_1(r_1u)Y_0(\kappa r_1 u)Y_0(ru) - Y_1(r_1u)Y_0(\kappa r_1 u)J_0(ru)] \tag{14}$$

$$A_2(u,r) = \sqrt{\frac{S_2T_2}{S_1T_1}}[Y_0(r_1u)J_1(\kappa r_1 u)J_0(ru) - J_0(r_1u)J_1(\kappa r_1 u)Y_0(ru)] - [Y_1(r_1u)J_0(\kappa r_1 u)J_0(ru) - J_1(r_1u)J_0(\kappa r_1 u)Y_0(ru)] \tag{15}$$

$$B_1(u) = \sqrt{\frac{S_2T_2}{S_1T_1}}[J_0(r_1u)Y_1(\kappa r_1 u)Y_0(r_w u) - Y_0(r_1u)Y_1(\kappa r_1 u)J_0(r_w u)] - [J_1(r_1u)Y_0(\kappa r_1 u)Y_0(r_w u) - Y_1(r_1u)Y_0(\kappa r_1 u)J_0(r_w u)] \tag{16}$$

and

$$B_2(u) = \sqrt{\frac{S_2T_2}{S_1T_1}}[Y_0(r_1u)J_1(\kappa r_1 u)J_0(r_w u) - J_0(r_1u)J_1(\kappa r_1 u)Y_0(r_w u)] - [Y_1(r_1u)J_0(\kappa r_1 u)J_0(r_w u) - J_1(r_1u)J_0(\kappa r_1 u)Y_0(r_w u)] \tag{17}$$

where $\kappa = \sqrt{T_1S_2/T_2S_1}$, $J_0(\cdot)$ and $Y_0(\cdot)$ are, respectively, the Bessel functions of the first and second kinds of order zero, and $J_1(\cdot)$ and $Y_1(\cdot)$ are, respectively, the Bessel functions of the first and second kinds of order one. Equations (12) and (13) are the closed-form solutions of hydraulic heads within the patch and outer regions. Detailed derivation for the solution is given in Appendix A.

2.3. Dimensionless variables

As a mean of expressing the solution in dimensionless form, the following dimensionless variables are defined: $\alpha = T_2/T_1$, $\beta = S_2/S_1$, $\tau = T_2t/S_2r_w^2$, $\rho = r/r_w$, $\rho_1 = r_1/r_w$, $\bar{h}_{D1} = \bar{h}_1/h_w$, $\bar{h}_{D2} = \bar{h}_2/h_w$, $h_{D1} = h_1/h_w$, and $h_{D2} = h_2/h_w$ where α represents the ratio of outer-region transmissivity to patch-region transmissivity (ratio of the transmissivity), β represents the ratio of outer-region storage coefficient to patch-region storage coefficient (ratio of storage coefficient), τ represents the dimensionless time during the test, ρ represents the dimensionless distance from the centre of well, ρ_1 represents the dimensionless thickness of the patch region, $\bar{h}_{D1}$ represents the dimensionless hydraulic head in the Laplace domain within the patch region, $\bar{h}_{D2}$ represents the dimensionless hydraulic head in the Laplace domain within the outer region, h_{D1} represents the dimensionless hydraulic head in the time domain within the patch region, and h_{D2} represents the dimensionless hydraulic head in the time domain within the outer region.

DOI: 10.1002/nag

The Laplace-domain solutions of (8) and (9) on dimensionless hydraulic head in a patchy aquifer are, respectively,

$$\bar{h}_{D1} = \frac{1}{p}\frac{\phi_1 I_0(q_1\rho) - \phi_2 K_0(q_1\rho)}{\phi_1 I_0(q_1) - \phi_2 K_0(q_1)} \tag{18}$$

and

$$\bar{h}_{D2} = \frac{1}{p}\frac{[\phi_1 I_0(q_1\rho_1) - \phi_2 K_0(q_1\rho_1)]K_0(q_2\rho)}{[\phi_1 I_0(q_1) - \phi_2 K_0(q_1)]K_0(q_2\rho_1)} \tag{19}$$

Accordingly, (12) and (13) can also be, respectively, expressed in dimensionless form as

$$h_{D1} = 1 + \frac{2}{\pi}\int_0^\infty \mathrm{e}^{-\beta\tau w^2/\alpha}\frac{[A_{D1}(w,\rho)B_{D2}(w) - A_{D2}(w,\rho)B_{D1}(w)]}{[B_{D1}^2(w) + B_{D2}^2(w)]}\frac{\mathrm{d}w}{w} \tag{20}$$

and

$$h_{D2} = 1 - \frac{4}{\pi^2\rho_1}\int_0^\infty \mathrm{e}^{-\beta\tau w^2/\alpha}\frac{[J_0(\kappa\rho w)B_{D1}(w) + Y_0(\kappa\rho w)B_{D2}(w)]}{[B_{D1}^2(w) + B_{D2}^2(w)]}\frac{\mathrm{d}w}{w^2} \tag{21}$$

where $w = r_w u$,

$$\begin{aligned} A_{D1}(w,\rho) = \sqrt{\alpha\beta}&[J_0(\rho_1 w)Y_1(\kappa\rho_1 w)Y_0(\rho w) - Y_0(\rho_1 w)Y_1(\kappa\rho_1 w)J_0(\rho w)] \\ &- [J_1(\rho_1 w)Y_0(\kappa\rho w)Y_0(\rho w) - Y_1(\rho_1 w)Y_0(\kappa\rho_1 w)J_0(\rho w)] \end{aligned} \tag{22}$$

$$\begin{aligned} A_{D2}(w,\rho) = \sqrt{\alpha\beta}&[Y_0(\rho_1 w)J_1(\kappa\rho_1 w)J_0(\rho w) - J_0(\rho_1 w)J_1(\kappa\rho_1 w)Y_0(\rho w)] \\ &- [Y_1(\rho_1 w)J_0(\kappa\rho_1 w)J_0(\rho w) - J_1(\rho_1 w)J_0(\kappa\rho_1 w)Y_0(\rho w)] \end{aligned} \tag{23}$$

$$\begin{aligned} B_{D1}(w) = \sqrt{\alpha\beta}&[J_0(\rho_1 w)Y_1(\kappa\rho_1 w)Y_0(w) - Y_0(\rho_1 w)Y_1(\kappa\rho_1 w)J_0(w)] \\ &- [J_1(\rho_1 w)Y_0(\kappa\rho_1 w)Y_0(w) - Y_1(\rho_1 w)Y_0(\kappa\rho_1 w)J_0(w)] \end{aligned} \tag{24}$$

and

$$\begin{aligned} B_{D2}(w) = \sqrt{\alpha\beta}&[Y_0(\rho_1 w)J_1(\kappa\rho_1 w)J_0(w) - J_0(\rho_1 w)J_1(\kappa\rho_1 w)Y_0(w)] \\ &- [Y_1(\rho_1 w)J_0(\kappa\rho_1 w)J_0(w) - J_1(\rho_1 w)J_0(\kappa\rho_1 w)Y_0(w)] \end{aligned} \tag{25}$$

The aquifer properties are constant through the whole aquifer if the aquifer is homogeneous. Accordingly, both α and β are equal to unity and the variables q_1 and q_2 in (18) and (19), respectively, are set to equal q. The Laplace-domain solutions of (18) and (19) reduce to the solution for a uniform formation as

$$\bar{h}_D = \frac{1}{p}\frac{K_0(q\rho)}{K_0(q)} \tag{26}$$

In addition, the solutions of (20) and (21) describing the dimensionless hydraulic head distributions can then algebraically reduce to

$$h_D(\tau,\rho) = 1 - \frac{2}{\pi}\int_0^\infty \mathrm{e}^{-\tau w^2}\frac{[J_0(w)Y_0(\rho w) - Y_0(w)J_0(\rho w)]}{[J_0^2(w) + Y_0^2(w)]}\frac{\mathrm{d}w}{w} \tag{27}$$

DOI: 10.1002/nag

Notably, (27) is identical to the solution given in Reference [10, p. 335, (6)] for a heat conduction problem. Equation (27), or in a slightly different form, can also be seen in some engineering applications, e.g. Goldstein [11] in a viscous fluid problem; Carslaw and Jaeger [12], Harvard's problem report [13], and Jaeger [14] in the heat conduction problems; Hantush [15] in the groundwater problem. Peng *et al.* [16] presented an efficient numerical approach to evaluate (27) with accuracy to five decimal places and for very wide ranges of dimensionless distances and times.

3. NUMERICAL STUDY

3.1. Curves of the integrand

The patchy aquifer system will reduce to a homogenous (uniform) aquifer system if $\alpha = 1$ (i.e. $T_1 = T_2$). In contrast, the aquifer has $T_1 > T_2$ for $\alpha < 1$ and $T_1 < T_2$ for $\alpha > 1$. In the following discussion, the ratio of storage coefficient β and dimensionless time τ are chosen as one. Figures 2(a)–(c) show the curves of integrands in (20) and (21) against the argument w for $\rho_1 = 3$ ($r_1 = 3r_w$) and $\alpha = 0.1$, 1 and 10 when $\tau = 1$. Figures 2(a) and (b) demonstrate the plots of integrand in (20) for $\rho = 2$ ($r = 2r_w$) and 3. Within the patch region (i.e. $1 \leqslant \rho \leqslant \rho_1$), the curve contains infinite sinuous waves and has the same roots for various values of α. When $\alpha \leqslant 1$, the curve of integrand is smooth since the amplitudes of oscillatory waves after the first zero-root are all smaller than 10^{-45}. The amplitude of the wave increases with α but for larger w the amplitude and tends toward zero. Note that each wave has two peaks for the case with $\alpha < 1$ and $\rho \leqslant 3$. Figure 2(b) shows that the sinuous waves of integrand in (21) for $\rho = 10$ when $\alpha = 0.1$, 1 or 10. As α increases the waves decrease in amplitude but increase in wavelength.

Figure 3 is an analysis of the effect of different sizes of patch regions, i.e. $\rho_1 = 3$ and 5 and $\alpha = 0.1$ and 10, for $\rho = 10$ when $\tau = 1$. The roots on the integrand for $\rho_1 = 3$ are slight smaller than those for $\rho_1 = 5$ if $\alpha = 0.1$. On the contrary, the roots for $\rho_1 = 3$ are slight larger than those for $\rho_1 = 5$ if $\alpha = 10$. The patch regions change from 3 to 5; consequently, the roots shift slightly along the dimensionless distance. Obviously, the differences of the roots are not apparent for the different sizes of patch regions. Thus, the thickness of the patchy region has significant effect on the integrands. Figures 2 and 3 demonstrate the patterns of curves that are helpful in obtaining the roots of integrands which will be used when (20) and (21) are computed numerically.

3.2. Numerical integrations

The improper integrals of (20) and (21) cannot be directly evaluated due to the complexity of both the Bessel functions and their products terms appeared in integrands. Each integral is transformed as a sum of infinite series and each term of series represents an area under the integrand and between two consecutive roots. The roots of integrand can be obtained by a root-search scheme along a horizontal axis [16]. The Shanks method [17] is applied to accelerate the convergence when evaluating the infinite series.

In a root-search scheme, an initial guess value is required to approximate the roots of the integrand along the w-axis. For $\rho > 1$ a reasonable step size for a uniform solution is $\Delta = \pi/(\rho - 1)$, [13]. This is also an appropriate choice for a patchy-aquifer solution when ρ is small, choosing the step size as Δ results in a good approximation for the first few roots of integrands in (20) and (21). The first root, w_1, is then approximated by $\pi/(\rho - 1)$. Therefore, the

DOI: 10.1002/nag

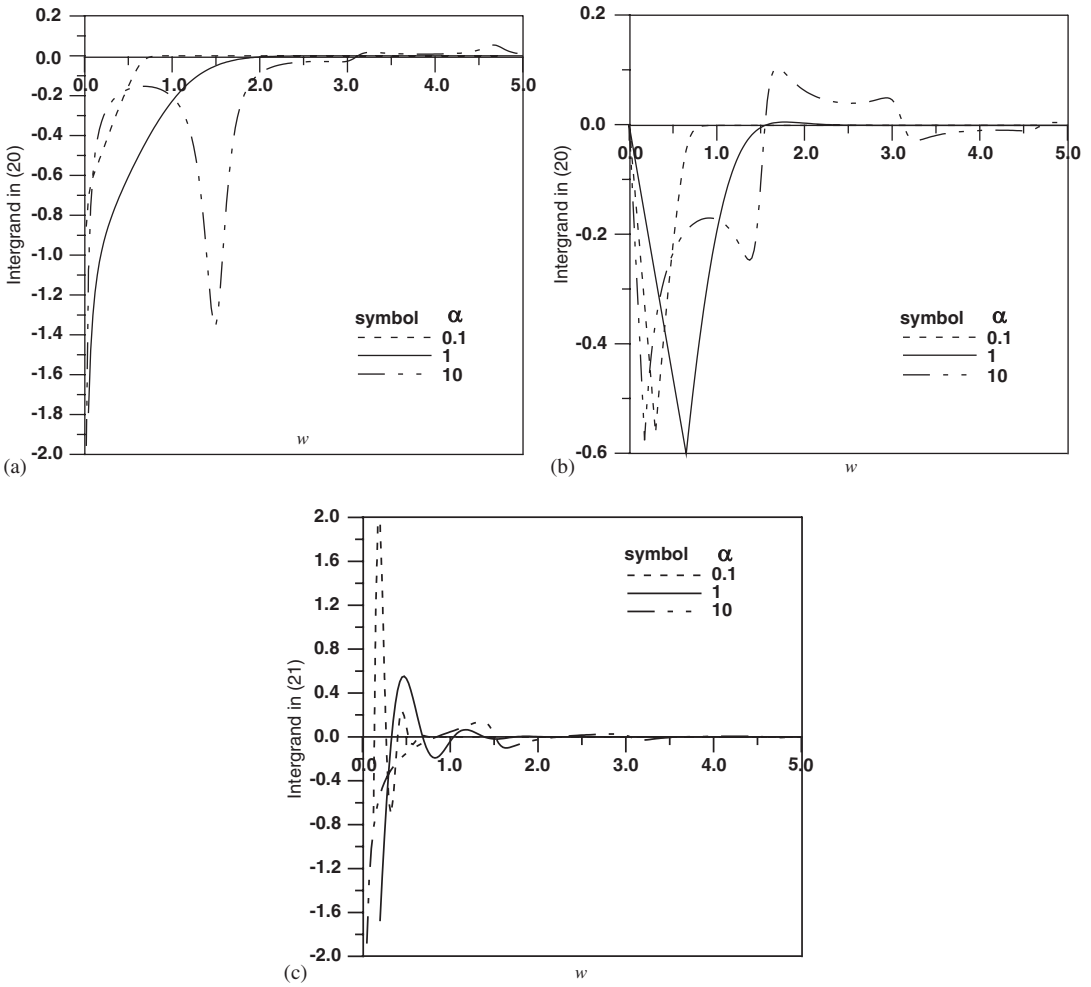

Figure 2. Plots of integrands in (20) and (21) versus w for $\tau = 1$ and $\alpha = 0.1$, 1 and 10 when: (a) $\rho = 2$; (b) $\rho = 3$; and (c) $\rho = 10$.

step size Δ_1 from the origin to the first root approximately equals $\pi/(\rho - 1)$. However, using the step size Δ_1 to estimate the large roots of the integrand will be very poor when ρ is large. Thus, a different approach for determining the step size is needed for large ρ. A reasonable approach for the second step size is chosen $\Delta_2 = w_1$, and the second root w_2 is approximately equal to $2w_1$. Similarly, the remaining step sizes Δ_i are chosen as $w_{i-1} - w_{i-2,}$ and the remaining roots are approximately equal to $w_i = w_{i-1} + \Delta_i$ where $i = 3, 4, \ldots$.

The integrands in (20) and (21) are oscillatory functions as displayed in Figures 2(a)–(c). A curve with double-peak waves can be observed for the case with $\alpha > 1$ and $1 \leqslant \rho \leqslant \rho_1$; in contrary, a curve with single-peak waves can be seen for the case that $\rho > \rho_1$. Obviously, the roots for the case with double peaks are difficult to obtain by the conventional root-search approaches such as Newton's method. The bisection method may be slow in convergence when

DOI: 10.1002/nag

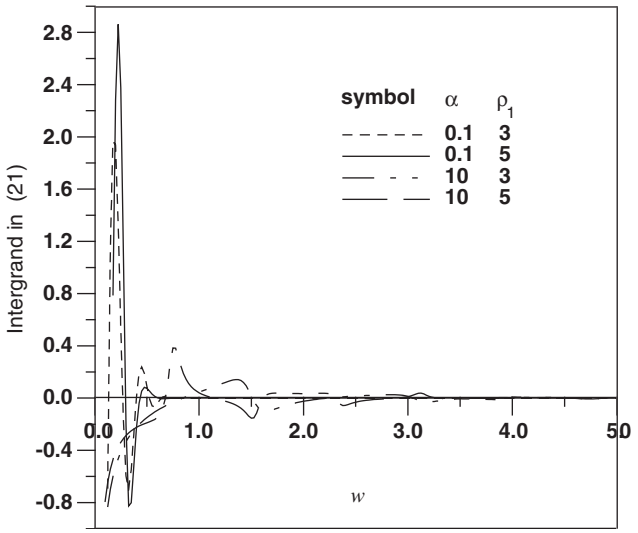

Figure 3. Plots of integrand in (21) versus w for $\tau = 1$, $\rho = 10$, and $\alpha = 0.1$ and 1 when the patch region $\rho_1 = 3$ or 5.

employing to obtain the roots, yet the advantage of this method is that it is guaranteed to work [18]. The bisection method is thus adopted to obtain the sequent roots of integrands in this study. The initial step size is chosen as $\Delta_i/10$ for the ith root to ensure that the first guess root ($w_i^1 = w_{i-1} + \Delta_i/10$) is smaller than the target root (w_i). The integrands in (20) and (21), $F(w_i)$, are evaluated in a forward direction (i.e. $w_i^k = w_{i-1} + k\Delta_i/10$, $k = 1, 2, \ldots$) until the condition $F(w_i^k) \cdot F(w_i^{k+1}) < 0$ is met to ensure that a target root lies between w_i^k and w_i^{k+1}. The bisection procedure is applied to search each root successively until the criterion $F(w_i) < 10^{-20}$ is met.

The values of integrands in (20) and (21) become infinity as w close to zero and approach zero for large w as indicated in Figures 2(a)–(c). Apparently, (20) and (21) are not easy to accurately evaluate especially when w is very close to the origin (singular point). Harvard's problem report [13] provided an approach when $\alpha = 1$ using an infinite series expansion to remove the singularity of integrand at the origin. Their approach can evaluate the integrand with good accuracy for a uniform aquifer system when w contains a singular point. However, their approach does not work in removing the singularity when $\alpha \neq 1$. Thus, the following approach using small increment is proposed in the evaluations of (20) and (21). Let ε be a very small value, say 10^{-20}. Starting from ε, the Gaussian quadrature [18] is employed to perform the numerical integration for (20) and (21) piecewise along the w-axis. The distance between two adjacent roots of integrand is divided into several small step sizes. Within each step, both the six-term and ten-term formulas of the Gaussian quadrature are used to carry out the integration for the same area under the integrand. The integration results after applying the six-term and ten-term formulas within a small step size are, respectively, defined as A_6 and A_{10}. The absolute difference of these two results is defined as $\Delta A = |A_{10} - A_6|$. If $\Delta A > 10^{-7}$, a half-step size ($\Delta w/2$) will be used and the same integration procedure will be repeatedly applied until $\Delta A < 10^{-7}$. If $\Delta A < 10^{-7}$, the same step size (Δw) is used when $10^{-8} \leqslant \Delta A \leqslant 10^{-7}$, otherwise, a double step size ($2\Delta w$) is used (i.e. $\Delta A < 10^{-8}$) for next step. This procedure ensures that each integration

DOI: 10.1002/nag

result over a small step has the accuracy at least to seven decimal places. The initial step size, Δw_i, for evaluating (20) and (21) is chosen as $(w_i - w_{i-1})/2$. The proposed integration procedure is adopted over the w-axis. Note that the last step size should be chosen such that the end of the step should be located right at a larger root. In short, the area between any two adjacent roots, which represents a term of infinite series, is obtained simply by adding the sum of the integration results form those small steps within the roots. Finally, the evaluation of infinite series may have the problem of slow convergence. Therefore, we employ the Shanks method to accelerate the convergence when evaluating the summation of alternating series.

4. RESULTS

Because of no published information on the storage coefficient of patchy aquifer, several investigators (e.g. References [2, 5, 19]) assumed that the storage coefficients of the patch and outer regions are the same to simplify the problems. Accordingly, dimensionless storage, β, is set as unity in this study. Equations (20) and (21), the time-domain solutions, are evaluated by the proposed approach. In addition, all evaluations are conducted in double-precision format and the convergence criterion for the Shanks method is chosen as 10^{-5}. The curves of dimensionless hydraulic head versus dimensionless time are developed to investigate the influences of the patchy aquifer properties and thickness on the hydraulic head distribution in a patchy aquifer system.

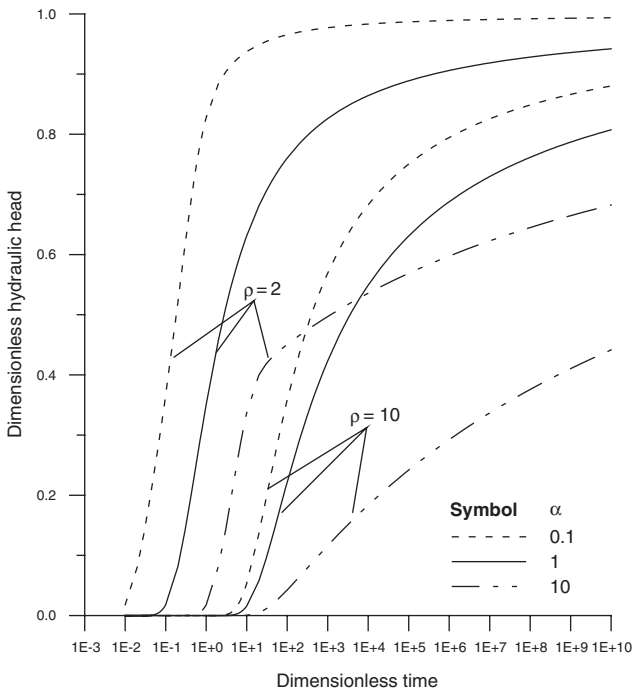

Figure 4. The effect of hydrogeological properties in the patch region on the shape of curves for $\rho_1 = 3$ and $\rho = 2$ and 10 when $\alpha = 0.1$, 1 or 10.

DOI: 10.1002/nag

Figure 4 exhibits the curves of dimensionless hydraulic head versus dimensionless time for $\rho_1 = 3$ and $\rho = 2$ and 10 when $\alpha = 0.1$, 1 or 10. Note that the dimensionless thickness of the patch region is equal to $\rho_1 - 1$. At either $\rho = 2$ or $\rho = 10$, the case of $\alpha = 0.1$ yields the highest dimensionless hydraulic head, the case of $\alpha = 1$ the second highest, and the case of $\alpha = 10$ the lowest under the same dimensionless time. Lower transmissivity in the patch region produces lower flow rate toward the outer region during the well test and results in smaller dimensionless hydraulic head in the patch and outer regions. On the other hand, larger transmissivity in the patch region yields larger flow rate across the wellbore and results in larger dimensionless heads in the patch and outer regions. Table I depicts the ratio of the dimensionless patch-aquifer hydraulic head to the dimensionless single-aquifer hydraulic head when the dimensionless thickness of the patch region, ρ_1, equals 3. At $\rho = 2$, the ratio may reach 1.48 if $\alpha = 0.1$ and 0.53 if $\alpha = 10$ when dimensionless time is very small (say, $\tau = 10$); on the other hand, the ratio is 1.05 if $\alpha = 0.1$ and 0.72 if $\alpha = 10$ when dimensionless time is very large (say, $\tau \geqslant 10^{10}$). In addition, at $\rho = 10$, the ratio may reach 3.41 if $\alpha = 0.1$ and 0.03 if $\alpha = 10$ when $\tau = 10$; in contrast, the ratio is 1.09 for $\alpha = 0.1$ and 0.55 for $\alpha = 10$ when $\tau \geqslant 10^{10}$. Those results demonstrate that the difference of dimensionless hydraulic heads between the patch and outer regions for $\alpha > 1$ is larger than that for $\alpha < 1$, especially the dimensionless time is very small.

Figure 5 displays the plot of dimensionless hydraulic head versus dimensionless distance for $\rho_1 = 3$ and $\tau = 1,\ 10^2,\ 10^4$ and 10^6 when $\alpha = 0.1$ or 10. This figure demonstrates the effects of the hydrogeological properties of the patch region on the shape of curves of the dimensionless hydraulic head. The head increases with dimensionless time in both the patch and outer regions; contrarily, the head decreases with increasing dimensionless radial distance. Note that Figure 5 indicates that the dimensionless hydraulic head for $\alpha = 0.1$ case is about 2.72 times to that for $\alpha = 10$ case at dimensionless large time (e.g. $\tau \geqslant 10^6$) when the dimensionless distance (ρ) equals 10. At the interface of the patch and outer regions (i.e. $\rho = \rho_1 = 3$), the slopes of curves

Table I. The ratio of dimensionless patch-aquifer hydraulic head to dimensionless single-aquifer hydraulic head for $\rho_1 = 3$ and $\rho = 2$ and 10 when $\alpha = 0.1$ or 10.

	$\rho = 2$		$\rho = 10$	
τ	$h_{D,0.1:1}$	$h_{D,10:1}$	$h_{D,0.1:1}$	$h_{D,10:1}$
1.0E + 01	1.48	0.53	3.41	0.03
1.0E + 02	1.27	0.59	1.62	0.19
1.0E + 03	1.18	0.60	1.34	0.27
1.0E + 04	1.14	0.62	1.24	0.33
1.0E + 05	1.11	0.64	1.19	0.38
1.0E + 06	1.09	0.66	1.16	0.42
1.0E + 07	1.08	0.68	1.13	0.46
1.0E + 08	1.07	0.69	1.11	0.49
1.0E + 09	1.06	0.71	1.10	0.52
1.0E + 10	1.05	0.72	1.09	0.55

Note that $h_{D,0.1:1}$ denotes the ratio of dimensionless hydraulic head when $\alpha = 0.1$ to dimensionless aquifer hydraulic head when $\alpha = 1$; $h_{D,10:1}$ denotes the ratio of dimensionless hydraulic head when $\alpha = 10$ to dimensionless aquifer hydraulic head when $\alpha = 1$.

DOI: 10.1002/nag

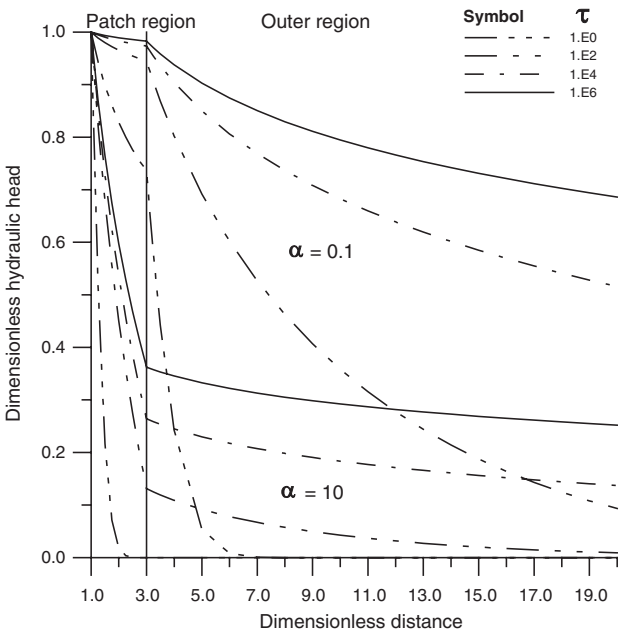

Figure 5. A plot of dimensionless hydraulic head versus dimensionless distance for $\rho_1 = 3$ and $\tau = 1$, 10^2, 10^4 and 10^6 when $\alpha = 0.1$ or 10.

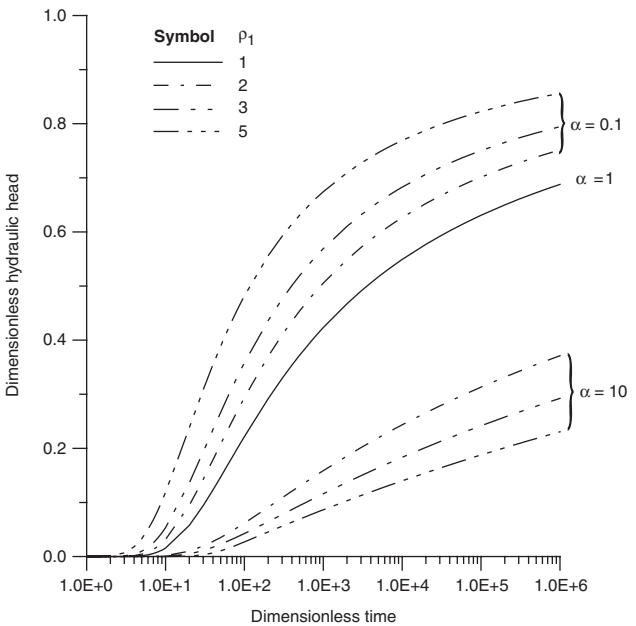

Figure 6. The curves of dimensionless hydraulic head versus dimensionless time for $\rho = 10$ and ρ_1 ranges from 1 (uniform aquifer) to 5 when $\alpha = 0.1$ or 10.

DOI: 10.1002/nag

are markedly different because of the contrast of transmissivity between the patch and outer regions. When $\alpha<1$, the slope of curve within the patch region is obviously smaller than that within the outer region due to the fact of larger transmissivity of the patch region demonstrated in Figure 5. In contrast, the slope of curve within a patch region is larger than that within the outer region when $\alpha > 1$. Obviously, the presence of the patch region influences the hydraulic head distribution in a patchy aquifer.

The effect of the patch-region thickness on dimensionless hydraulic head distribution is depicted in Figure 6 where the curves are plotted against dimensionless time at $\rho = 10$ and dimensionless thickness of the patch region (ρ_1) ranging from 2 to 5 when $\alpha = 0.1$, 1 or 10. This figure demonstrates that increasing dimensionless patch-region thickness increases dimensionless hydraulic head for $\alpha = 0.1$ and decreases dimensionless hydraulic head for $\alpha = 10$.

5. CONCLUSIONS

The mathematical model describing the radial groundwater flow in a confined patchy aquifer system is present for well constant-head tests. The closed-form solution expressed in term of hydraulic head is derived by the Laplace transforms and the Bromwich integral method. In addition, we also have proven that the solution satisfies the governing equations, boundary conditions, and continuity requirements at the interface of the patch and outer regions. An efficient numerical approach is proposed to evaluate the solution. The numerical approach includes a root-search scheme for finding the consecutive roots of integrand, the Gaussian quadrature for performing the numerical integration, and the Shanks method for accelerating the convergence when evaluating the Bessel functions and the alternating infinite series transformed from the integral. Finally, the influences of the properties and thickness of the patch region on dimensionless hydraulic head distribution are explored. This new time-domain solution can be used for identifying the aquifer parameters, verifying the numerical code, or studying the effect of the contrast of the formation properties on the hydraulic head distribution. Three conclusions are drawn as follows:

1. The effect of hydraulic head in a patchy aquifer system for $T_1 < T_2$ is larger than that for $T_1 > T_2$. At $\rho = 2$, the ratio may reach 1.48 if $\alpha = 0.1$ and 0.53 if $\alpha = 10$ when dimensionless time is very small; on the other hand, the ratio is 1.05 if $\alpha = 0.1$ and 0.72 if $\alpha = 10$ when dimensionless time is very large. In addition, at $\rho = 10$, the ratio may reach 3.41 if $\alpha = 0.1$ and 0.03 if $\alpha = 10$ when dimensionless time is very small; in contrast, the ratio is 1.09 for $\alpha = 0.1$ and 0.55 for $\alpha = 10$ when dimensionless time is very large.
2. The presence of the finite-thickness patch region around a test well substantially influences the shape of hydraulic head distribution. The curve developed for the case with a finite thickness of the patch region shows an abrupt change in slope at the interface of the patch and outer regions. This indicates that the hydraulic head distribution depends on the hydraulic properties of both the patch and outer regions.
3. The thickness of the patch region significantly affects the distribution of dimensionless hydraulic head in a patchy aquifer system. The dimensionless hydraulic head for $\alpha = 0.1$ case is about 2.72 times to that for $\alpha = 10$ case at dimensionless large time (e.g. $\tau \geqslant 10^6$) when the dimensionless distance (ρ) equals 10. It is to conclude that a thicker patch region give higher hydraulic head when $T_1 > T_2$ and lower hydraulic head when $T_1 < T_2$.

DOI: 10.1002/nag

APPENDIX A: DERIVATIONS OF (12) AND (13)

The inverse Laplace transforms of (8) and (9) in the time domain can be obtained by using the Laplace inversion integral [9] as

$$h_1 = \frac{1}{2\pi \mathrm{i}} \int_{a-\mathrm{i}\infty}^{a+\mathrm{i}\infty} \mathrm{e}^{pt} \bar{h}_1 \, \mathrm{d}p \tag{A1}$$

and

$$h_2 = \frac{1}{2\pi \mathrm{i}} \int_{a-\mathrm{i}\infty}^{a+\mathrm{i}\infty} \mathrm{e}^{pt} \bar{h}_2 \, \mathrm{d}p \tag{A2}$$

where p is a complex variable and a is a large, real, positive constant, so much so that all the poles lie to the left of line $(a - \mathrm{i}\infty, a + \mathrm{i}\infty)$.

The integrands in (8) and (9) contains a branch point at $p = 0$ on the cut plane. Thus, these integrations may require the usage of the Bromwich contour integrals for the Laplace inversion. The closed contour of integrand is shown in Figure A1 with a cut along the negative real axis, where δ is a small positive number.

A single branch point with a singularity (pole) at $p = 0$ exists in the integrand in (8). Accordingly, this integration can be carried out by the use of contour integral. The integrals taken along BCD and GHA tend to zero as $R \to \infty$. Consequently, (8) can be superseded by the sum of integrals along DE and FG, and the small circle EF around the origin as $\delta \to 0$. In other words, the integral can then be written as

$$h_1 = \lim_{\substack{\delta \to 0 \\ R \to \infty}} \frac{1}{2\pi \mathrm{i}} \left[\int_{EF} \mathrm{e}^{pt} \bar{h}_1 \, \mathrm{d}p + \int_{DE} \mathrm{e}^{pt} \bar{h}_1 \, \mathrm{d}p + \int_{FG} \mathrm{e}^{pt} \bar{h}_1 \, \mathrm{d}p \right] \tag{A3}$$

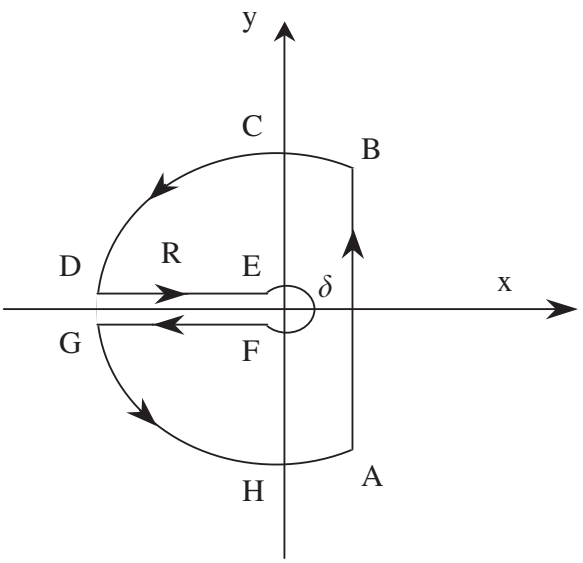

Figure A1. A plot of the closed-contour integration of the $\bar{h}_1$ and $\bar{h}_2$ as a function of $p = x + yi$ for calculating the inverse Laplace transform.

DOI: 10.1002/nag

Along the small circle EF as $\delta \to 0$, introducing the limiting form into the first term on the right-hand side (RHS) of (A3) obtains

$$h_{11} = \lim_{p\to 0} p\left[\frac{h_w}{p}\frac{\phi_1 I_0(q_1 r) - \phi_2 K_0(q_1 r)}{\phi_1 I_0(q_1 r_w) - \phi_2 K_0(q_1 r_w)}\right] \tag{A4}$$

As $p \to 0$, q_1 and q_2 approach to zero. Thus, $I_0(0)$ and $I_1(0)$ approach one and zero, respectively, and $K_0(0)$ and $K_1(0)$ become indefinite. The result of (A4) can be obtained as

$$h_{11} = h_w \tag{A5}$$

For the second term on the RHS of (A3) along DE, we introduce the change of variable $p = u^2 e^{-\pi i} T_1/S_1$, and use the formulas [10, p. 490, (25) and (26)]

$$K_v(z e^{\pm(1/2)\pi i}) = \pm \tfrac{1}{2}\pi i e^{\mp(1/2)v\pi i}[-J_v(z) \pm i Y_v(z)] \tag{A6}$$

and

$$I_v(z e^{\pm(1/2)\pi i}) = e^{\pm(1/2)v\pi i} J_v(z) \tag{A7}$$

where $v = 0, 1, 2, \ldots$. The second term on the RHS of (A3) leads to

$$h_{12} = -\frac{h_w}{\pi i}\int_0^\infty e^{-(T_1/S_1)u^2 t}\frac{A_1(u) + iA_2(u)}{B_1(u) + iB_2(u)}\frac{du}{u} \tag{A8}$$

Likewise, introducing $p = u^2 e^{\pi i} T_1/S_1$, the integral along EF gives minus the conjugate of (A8) as

$$h_{13} = \frac{h_w}{\pi i}\int_0^\infty e^{-(T_1/S_1)u^2 t}\frac{A_1(u) - iA_2(u)}{B_1(u) - iB_2(u)}\frac{du}{u} \tag{A9}$$

The closed-form solution of (12) can then be obtained by combining (A5), (A8), and (A9). Also, the closed-form solution of (13) can be obtained in a similar manner.

APPENDIX B: PROOF OF THE CLOSED-FORM SOLUTION

This section gives the proof that the time-domain solution satisfies the governing equation, boundary conditions, and continuity requirements at the interface of the patch and outer regions. For the outer boundary, $r \to \infty$, one has $J_1(\infty) = 0$ and $Y_1(\infty) = 0$. Taking the derivative of (13) with respect to r and letting $r \to \infty$ gives

$$\left.\frac{\partial h_2}{\partial r}\right|_{r\to\infty} = -\frac{4h_w}{\pi^2 r_1}\int_0^\infty e^{-(T_1/S_1)u^2 t}\frac{[-\kappa u J_1(\infty)B_1(u) - \kappa u Y_1(\infty)B_2(u)]}{[B_1^2(u) + B_2^2(u)]}\frac{du}{u^2}$$
$$= 0 \tag{B1}$$

Therefore, the outer boundary condition of (4) is satisfied.

When $r = r_w$, $A_1(u, r_w) = B_1(u)$ and $A_2(u, r_w) = B_2(u)$; consequently, the integrand in (12) becomes zero. Thus, one obtains the result of (5) which is the boundary condition for maintaining a constant head around the well.

Letting $r = r_1$ and using the formula [12]

$$J_1(u)Y_0(u) - J_0(u)Y_1(u) = 2/(\pi u) \tag{B2}$$

DOI: 10.1002/nag

Equations (14) and (15), respectively, become

$$A_1(u,r_1) = -[J_1(r_1u)Y_0(r_1u) - Y_1(r_1u)J_0(r_1u)]Y_0(\kappa r_1u)$$
$$= \frac{-2}{\pi r_1 u} Y_0(\kappa r_1 u) \tag{B3}$$

and

$$A_2(u,r_1) = [J_1(r_1u)Y_0(r_1u) - Y_1(r_1u)J_0(r_1u)]J_0(\kappa r_1u)$$
$$= \frac{2}{\pi r_1 u} J_0(\kappa r_1 u) \tag{B4}$$

Substituting (B3) and (B4) into (12) yields (13). Here we have shown the continuity of hydraulic head between the patch and outer regions.

Taking the derivatives of $A_1(u,r)$ and $A_2(u,r)$ with respect to r and letting $r = r_1$, respectively, gets

$$\left.\frac{\partial A_1(u,r)}{\partial r}\right|_{r=r_1} = \frac{2}{\pi r_1}\sqrt{\frac{S_2T_2}{S_1T_1}}\, Y_1(\kappa r_1 u) \tag{B5}$$

and

$$\left.\frac{\partial A_2(u,r)}{\partial r}\right|_{r=r_1} = \frac{-2}{\pi r_1}\sqrt{\frac{S_2T_2}{S_1T_1}}\, J_1(\kappa r_1 u) \tag{B6}$$

Furthermore, letting $r = r_1$ and multiplying by T_1 on both sides after taking the derivative of (12) with respect to r yields

$$T_1\left.\frac{\partial h_1}{\partial r}\right|_{r=r_1} = \frac{4h_w}{\pi^2 r_1}\sqrt{\frac{S_2T_1T_2}{S_1}}\int_0^\infty e^{-(T_1/S_1)u^2t}\frac{[J_1(\kappa r_1u)B_1(u) + Y_1(\kappa r_1u)B_2(u)]}{[B_1^2(u)+B_2^2(u)]}\frac{du}{u} \tag{B7}$$

Similarly, one can get

$$T_2\left.\frac{\partial h_2}{\partial r}\right|_{r=r_1} = \frac{4h_w}{\pi^2 r_1}\sqrt{\frac{S_2T_1T_2}{S_1}}\int_0^\infty e^{-(T_1/S_1)u^2t}\frac{[J_1(\kappa r_1u)B_1(u) + Y_1(\kappa r_1u)B_2(u)]}{[B_1^2(u)+B_2^2(u)]}\frac{du}{u} \tag{B8}$$

Therefore, we obtain

$$T_1\left.\frac{\partial h_1}{\partial r}\right|_{r=r_1} = T_2\left.\frac{\partial h_2}{\partial r}\right|_{r=r_1} \tag{B9}$$

Again, we have shown the continuity of flow rate between the patch and outer regions.

We can carry similar steps demonstrated above by taking the first and second derivatives with respect to r and the derivative with respect to t for (12) and (13) to prove that the time-domain solutions satisfy the governing equations, (1) and (2). McLachlan [20, pp. 192–197] gave the formulas

$$\frac{\partial J_0(ru)}{\partial r} = -uJ_1(ru) \tag{B10}$$

$$\frac{\partial J_1(ru)}{\partial r} = u\left[\frac{1}{ru}J_1(ru) - J_2(ru)\right] \tag{B11}$$

DOI: 10.1002/nag

and

$$\frac{2}{ru}J_1(ru) = J_2(ru) + J_0(ru) \tag{B12}$$

Similarly,

$$\frac{\partial Y_0(ru)}{\partial r} = -uY_1(ru) \tag{B13}$$

$$\frac{\partial Y_1(ru)}{\partial r} = u\left[\frac{1}{ru}Y_1(ru) - Y_2(ru)\right] \tag{B14}$$

and

$$\frac{2}{ru}Y_1(ru) = Y_2(ru) + Y_0(ru) \tag{B15}$$

Based on formulas (B10)–(B12), one can obtain

$$\frac{\partial^2 J_0(ru)}{\partial r^2} + \frac{1}{r}\frac{\partial J_0(ru)}{\partial r} = -u^2 J_0(ru) \tag{B16}$$

Likewise,

$$\frac{\partial^2 Y_0(ru)}{\partial r^2} + \frac{1}{r}\frac{\partial Y_0(ru)}{\partial r} = -u^2 Y_0(ru) \tag{B17}$$

After taking the first and second derivatives with respect to r for $A_1(u,r)$ and using formula (B17), one can get

$$\begin{aligned}\frac{\partial^2 A_1(u,r)}{\partial r^2} + \frac{1}{r}\frac{\partial A_1(u,r)}{\partial r} = \sqrt{\frac{S_2T_2}{S_1T_1}}&[J_0(r_1u)Y_1(\kappa r_1u)(-u^2Y_0(ru)) - Y_0(r_1u)Y_1(\kappa r_1u)(-u^2J_0(ru))]\\ &- [J_1(r_1u)Y_0(\kappa r_1u)(-u^2Y_0(ru)) - Y_1(r_1u)Y_0(\kappa r_1u)(-u^2J_0(ru))]\end{aligned} \tag{B18}$$

Applying (14) obtains

$$\frac{\partial^2 A_1(u,r)}{\partial r^2} + \frac{1}{r}\frac{\partial A_1(u,r)}{\partial r} = -u^2 A_1(u,r) \tag{B19}$$

Similarly, one can get

$$\frac{\partial^2 A_2(u,r)}{\partial r^2} + \frac{1}{r}\frac{\partial A_2(u,r)}{\partial r} = -u^2 A_2(u,r) \tag{B20}$$

Substituting (12) into (1) and using (B19) and (B20), the left-hand side of (1) yields

$$\frac{\partial^2 h_1}{\partial r^2} + \frac{1}{r}\frac{\partial h_1}{\partial r} = \frac{2h_w}{\pi}\int_0^\infty e^{-(T_1/S_1)u^2t}\frac{[-u^2A_1(u,r)]B_2(u) - [-u^2A_2(u,r)]B_1(u)}{[B_1^2(u) + B_2^2(u)]}\frac{du}{u} \tag{B21}$$

Taking the derivative of (12) with respect to t and multiplying by S_1/T_1, the RHS of (1) yields

$$\frac{S_1}{T_1}\frac{\partial h_1}{\partial t} = \frac{2h_w}{\pi}\int_0^\infty e^{-(T_1/S_1)u^2t}\frac{[-u^2A_1(u,r)]B_2(u) - [-u^2A_2(u,r)]B_1(u)}{[B_1^2(u) + B_2^2(u)]}\frac{du}{u} \tag{B22}$$

Since (B21) equals (B22), we have shown that the closed-form solution of (12) satisfies (1). Likewise, one can prove that (13) satisfies (2) also.

DOI: 10.1002/nag

ACKNOWLEDGEMENTS

This study was partly supported by the Taiwan National Science Council under grant NSC90-2621-Z-009-003. The writers appreciate the comments and suggested revisions of two anonymous reviewers that help improve the clarity of our presentation.

REFERENCES

1. Barker JA, Herbert R. Pumping tests in patchy aquifers. *Ground Water* 1982; **20**(2):150–155.
2. Novakowski KS. A composite analytical model for analysis of pumping tests affected by wellbore storage and finite thickness skin. *Water Resource Research* 1989; **25**(9):1937–1946.
3. Streltsova TD, McKinley RM. Effect of flow time duration on buildup pattern for reservoirs with heterogeneous properties. *Society of Petroleum Engineers Journal* 1984; **24**:294–306.
4. Streltsova TD. *Well Testing in Heterogeneous Formations*. Wiley: New York, 1988; 45–49.
5. Novakowski KS. Interpretation of the transient flow rate obtained from constant-head tests conducted in situ in clays. *Canadian Geotechnical Journal* 1993; **30**:600–606.
6. Markle JM, Rowe RK, Novakowski KS. A model for the constant-heat pumping test conducted in vertically fractured media. *International Journal for Numerical and Analytical Methods in Geomechanics* 1995; **19**:457–473.
7. Chang CC, Chen CS. Analysis of constant-head for a two-layer radially symmetric nonuniform model. *Proceeding of the Third Groundwater Resources and Water Quality Protection Conference*, National Central University, Chung-Li, Taiwan, 1999; 68–75.
8. Spiegel MR. *Laplace Transforms*. Schaum Publishing Co.: New York, 1965.
9. Hildebrand FB. *Advanced Calculus for Applications*. (2nd edn). Prentice-Hall: New York, 1976.
10. Carslaw HS, Jaeger JC. *Conduction of Heat in Solids* (2nd edn). Clarendon Press: Oxford, U.K., 1959.
11. Goldstein S. Some two-dimensional diffusion problems with circular symmetry. *Proceedings of the London Mathematical Society* (II) 1932; 51–88.
12. Carslaw HS, Jaeger JC. Some two-dimensional problems in conduction of heat with circular symmetry. *Some Problems in Conduction of Heat* 1939; **46**:361–388.
13. Harvard Problem Report. *A Function Describing the Conduction of Heat in a Solid Medium Bounded Internally by a Cylindrical Surface*. Computation Laboratory of Harvard University, 1950; **76**:1–18.
14. Jaeger JC. Numerical values for the temperature in radial heat flow. *Journal of Mathematical Physics* 1956; **34**: 316–321.
15. Hantush MS. Flow of ground water in sands of nonuniform thickness. Part I: Flow in wedge-shaped aquifer. *Journal of Geophysical Research* 1962; **67**(2):703–709.
16. Peng HY, Yeh HD, Yang SY. Improved numerical evaluation of the radial groundwater flow equation. *Advances in Water Resources* 2002; **25**(6):663–675.
17. Shanks D. Non-linear transformations of divergent and slowly convergent sequences. *Journal of Mathematical Physics* 1955; **34**:1–42.
18. Gerald CF, Wheatley PO. *Applied Numerical Analysis* (4th edn). Addison-Wesley: California, 1989.
19. Butler Jr JJ. Pumping tests in nonuniform aquifers—the radially symmetric case. *Journal of Hydrology* 1988; **101**: 15–30.
20. McLachlan NW. *Bessel Functions for Engineers* (2nd edn). Clarendon Press: Oxford, U.K., 1955.

DOI: 10.1002/nag